

RESEARCH ARTICLE

Flight muscle power increases with strain amplitude and decreases with cycle frequency in zebra finches (*Taeniopygia guttata*)

Joseph W. Bahlman^{1,*}, Vikram B. Baliga^{2,*} and Douglas L. Altshuler^{2,†}**ABSTRACT**

Birds that use high flapping frequencies can modulate aerodynamic force by varying wing velocity, which is primarily a function of stroke amplitude and wingbeat frequency. Previous measurements from zebra finches (*Taeniopygia guttata*) flying across a range of speeds in a wind tunnel demonstrate that although the birds modulated both wingbeat kinematic parameters, they exhibited greater changes in stroke amplitude. These two kinematic parameters contribute equally to aerodynamic force, so the preference for modulating amplitude over frequency may instead derive from limitations of muscle physiology at high frequency. We tested this hypothesis by developing a novel *in situ* work loop approach to measure muscle force and power output from the whole pectoralis major of zebra finches. This method allowed for multiple measurements over several hours without significant degradation in muscle power. We explored the parameter space of stimulus, strain amplitude and cycle frequencies measured previously from zebra finches, which revealed overall high net power output of the muscle, despite substantial levels of counter-productive power during muscle lengthening. We directly compared how changes to muscle shortening velocity via strain amplitude and cycle frequency affected muscle power. Increases in strain amplitude led to increased power output during shortening with little to no change in power output during lengthening. In contrast, increases in cycle frequency did not lead to increased power during shortening but instead increased counter-productive power during lengthening. These results demonstrate why at high wingbeat frequency, increasing wing stroke amplitude could be a more effective mechanism to cope with increased aerodynamic demands.

KEY WORDS: Pectoralis major, Work loop, Skeletal muscle, Bird flight

INTRODUCTION

Flying animals routinely perform locomotor behaviors that require adjustments to the aerodynamic force they produce. Behaviors such as accelerating and decelerating, maneuvering, changing altitude or carrying additional weight all require a flyer to produce a different amount of aerodynamic force from that for steady-state behavior. There are several mechanisms that flapping flyers can use to vary the

amount of aerodynamic force their wings produce but adjusting wing velocity has the most substantial effect because aerodynamic force varies as a function of velocity squared. During flapping flight, velocity at the wing is determined both by body velocity of the animal and by velocity due to wing flapping, which requires modulation of mechanical power output (e.g. Altshuler et al., 2010a; Bahlman et al., 2014; Jackson and Dial, 2011; Tobalske and Biewener, 2008; Tobalske et al., 2003). Velocity due to flapping at any given position along the wing (V_r) is the product of spanwise position along the wing (r) and two motion parameters: wingbeat amplitude (Φ) and wingbeat frequency (f) (Eqn 1). The two motion parameters scale the same with velocity and therefore contribute equally to aerodynamic force output (F_{Aero}) (Eqn 2) and power requirement (P_{Aero}) (Eqn 3):

$$V_r = r\Phi f, \quad (1)$$

$$F_{\text{Aero}} \propto \Phi^2 f^2, \quad (2)$$

$$P_{\text{Aero}} = F_{\text{Aero}} V_r \propto \Phi^3 f^3. \quad (3)$$

Moreover, aerodynamic force scales as the square of both amplitude and frequency, whereas mechanical power required scales with the cube. The exponential trends indicate that increasing wing velocity via an equal contribution from both motion parameters will require less mechanical power than if one parameter was increased more than the other.


Despite this aerodynamic equivalence, small birds with high wingbeat frequencies preferentially increase wingbeat amplitude over frequency during some performance challenges. Hummingbirds favor increases to stroke amplitude during sub-maximal load lifting (Mahalingam and Welch, 2013), with increasing speed (Tobalske et al., 2007) and in reduced air density (Altshuler and Dudley, 2003; Altshuler et al., 2010b; Chai and Dudley, 1996). The hummingbirds in these studies had wingbeat frequencies that ranged from ~40 to ~60 Hz. Zebra finches (*Taeniopygia guttata*), another small bird with high wingbeat frequency (~26–30 Hz), favor increasing stroke amplitude over wingbeat frequency when briefly hovering but favor increasing wingbeat frequency over amplitude when flying at increasing speeds in a wind tunnel (Ellerby and Askew, 2007b).

Because there is no aerodynamic explanation for preferring either wingbeat amplitude or frequency over the other, we hypothesize that observed preferences may be due to differences in a flight muscle's ability to produce power at high frequency. The structure of a bird's shoulder causes the wing's rotational motion to be tightly coupled to the contractile motion of two pectoral muscles: the pectoralis major and the supracoracoideus. The wingbeat frequency is equal to and determined by the frequency of the pectoral muscle contraction cycles. Similarly, the wing stroke amplitude, a rotational parameter (degrees) is proportional to the linear strain amplitude (millimeters) of the pectoralis muscle, though also influenced by the synergistic

¹Department of Biological Sciences, California State University, Sacramento, CA 95819, USA. ²Department of Zoology, University of British Columbia, Vancouver, BC, Canada, V6T 1Z4.

*These authors contributed equally to this work

†Author for correspondence (doug@zoology.ubc.ca)

 J.W.B., 0000-0002-7870-5479; V.B.B., 0000-0002-9367-8974; D.L.A., 0000-0002-1364-3617

activity of other muscles operating across the shoulder joint. Previous studies on cyclic contractions in mouse soleus have shown the force–velocity and force–length relationships will appear different under different conditions of stimulus, strain and frequency, and these differences will be accentuated at particularly high levels of strain and frequency (Askew and Marsh, 1998). Small birds use high wingbeat frequency during flapping flight, which means that their pectoral muscles have among the highest muscle cycle frequencies of any vertebrate skeletal muscle (Hagiwara et al., 1968), well beyond what is considered extreme for mouse soleus. The extreme values of muscle cycle frequency in small birds suggests that further increases in cycle frequency may be detrimental, thereby favoring increases in strain amplitude. We hypothesize that these birds use unequal increases in amplitude and frequency to produce additional aerodynamic force, because of limitations in the flight muscles' ability to produce mechanical power equally for the two parameters at already high baseline wingbeat frequencies.

Testing this hypothesis requires a method that allows us to systematically vary wing stroke amplitude and wingbeat frequency while measuring the flight muscle's mechanical power output. When applied *in vitro* or *in situ*, the work-loop approach (Josephson, 1985) allows for systematic and independent testing of how muscle strain, cycle frequency and activation parameters affect mechanical power output (Ahn, 2012). Within a cycle, the effects of stimulus duration, phase and strain amplitude on changes to net work can be seen by plotting force against position (Fig. 1A–D). Because changes to cycle frequency, and therefore the timing of force and work output, may not be readily apparent from work loops themselves, it is then beneficial to visualize the time course of instantaneous power (Fig. 1E). Determining how instantaneous power varies over the duration of each contraction cycle provides insight on the rate of change of muscle work output, which may be distinct between muscle lengthening and muscle shortening phases.

Because there are multiple features that determine muscle work and power, most of which can be manipulated in a work-loop experiment, there is a vast parameter space that can be explored. The specific goal of our study was to ask whether there is a difference in the muscle power output when increasing shortening velocity via strain amplitude versus cycle frequency. This question was motivated by an *in vivo* study of zebra finches (*Taeniopygia guttata*) flying in a wind tunnel at speeds from 0 to 14 m s⁻¹ (Ellerby and Askew, 2007a,b). During hovering flight (0 m s⁻¹), the zebra finches exhibited greater modulation of strain amplitude compared with cycle frequency, but they exhibited more equivalent changes to strain amplitude and frequency when flying at progressively faster speeds. Across these flight speeds, the pectoralis major muscle was activated for 13–16 ms per cycle, which spanned a range of electromyogram (EMG) duty cycles from ~33% to ~46%. The muscle was activated at an onset phase that ranged from 15% to 18% of the cycle prior to peak length. The fascicle strain (standardized to resting length) ranged from 13.3% to 16.4%, and the cycle frequency ranged from 26 to 30 Hz. We performed work-loop measurements over this parameter space to determine why wing stroke amplitude should be favored over wingbeat frequency.

Work-loop studies on a whole pectoralis muscle are challenging because the method requires fixing the proximal attachment of the muscle, which is widely distributed across a keeled sternum, a clavicle and several ribs. Previous studies using bird pectoralis major have used only isolated fiber bundles (Askew and Marsh, 2001; Ellerby and Askew, 2007a; Reiser et al., 2013), which cannot account for the muscle's unique multi-pennate architecture, central tendon or other whole-muscle properties. To overcome this challenge, we developed a

custom-fitted brace to immobilize the bird's entire thorax and therefore the proximal attachments of the muscle. This setup allowed us to actuate the humeral attachment of the pectoralis using sinusoidal strain, and to stimulate the muscle within the bird to perform *in situ* work-loop experiments. Six initial experiments were designed to determine the range of stimulus parameters (duration and phase) that yielded high net muscle power. We then built on this information to perform eight key experiments to determine how varying muscle strain and cycle frequency affected muscle power output.

MATERIALS AND METHODS

Animals

Twelve adult male zebra finches, *Taeniopygia guttata* (Vieillot 1817), were used for the experiments (Tables S1 and S2). Birds were obtained from commercial and university breeding facilities and housed in wire cages with *ad libitum* access to commercial seed mix and water under a 12 h:12 h light:dark cycle. All procedures were approved by the University of British Columbia Animal Care Committee.

Surgical setup

We used the work-loop technique (Josephson, 1985) to measure power output of whole pectoralis major muscles from zebra finches *in situ*. The surgery and attachment of muscle to the ergometer, implantation of stimulating electrodes and data collection were all done with the bird deeply anesthetized with isoflurane. It is known that isoflurane leads to decreased muscle force and prolonged relaxation in mammalian skeletal muscle (Kunst et al., 1999). It is unknown whether the same effect is present in birds, but similar levels of isoflurane (2–4%) were delivered throughout all trials.

Muscle length was controlled by securing the distal attachment of the pectoralis major to a servo motor, while the proximal attachment and the bird's entire thorax were immobilized in a custom brace. The brace was a 3D-printed, ABS plastic clamp with upper and lower surfaces contoured to match the bird's dorsal and ventral surfaces, respectively (part files are available from figshare: <https://doi.org/10.6084/m9.figshare.12520733>). The clamp was tightened with screws to compress the bird's thorax sufficiently and ensure that the contracting pectoralis would not further compress the thorax, causing the bird to slip out of the brace. The distal muscle attachment was prepared by severing the delto-pectoral crest from the humerus with a scalpel. The pectoralis major tendon is deep and not in series, so we attached the muscle directly to an ergometer (model 305C, Aurora Scientific Inc., Aurora, ON, Canada) by suturing one end of a non-compliant thermoplastic thread through the muscle and around the bone fragment and tying the other end to the lever of the ergometer. At both ends, the knots were sealed with cyanoacrylate to prevent slipping.

This approach allowed for the first *in situ* recordings of a whole avian pectoralis major muscle but cannot recreate the full complexity of *in vivo* strain. We used a sine wave trajectory, whereas *in vivo*, the relative duration of shortening is greater than lengthening. The muscle length was varied by imposing changes along the muscle's central axis, which does not account for the *in vivo* wrapping of the pectoralis major around the thorax or any level of rotation in the humerus. The *in vivo* strain measurements used to seed the experimental space were based on fascicle strains from a multipennate muscle whereas the ergometer imposed strains along the whole muscle's line of action. Another consequence of holding the muscle in place was that the brace caused some level of thoracic compression. We looked for but did not detect any change in resting breathing rate, but the brace likely constrained higher breathing rate such as occurs during strenuous exercise.

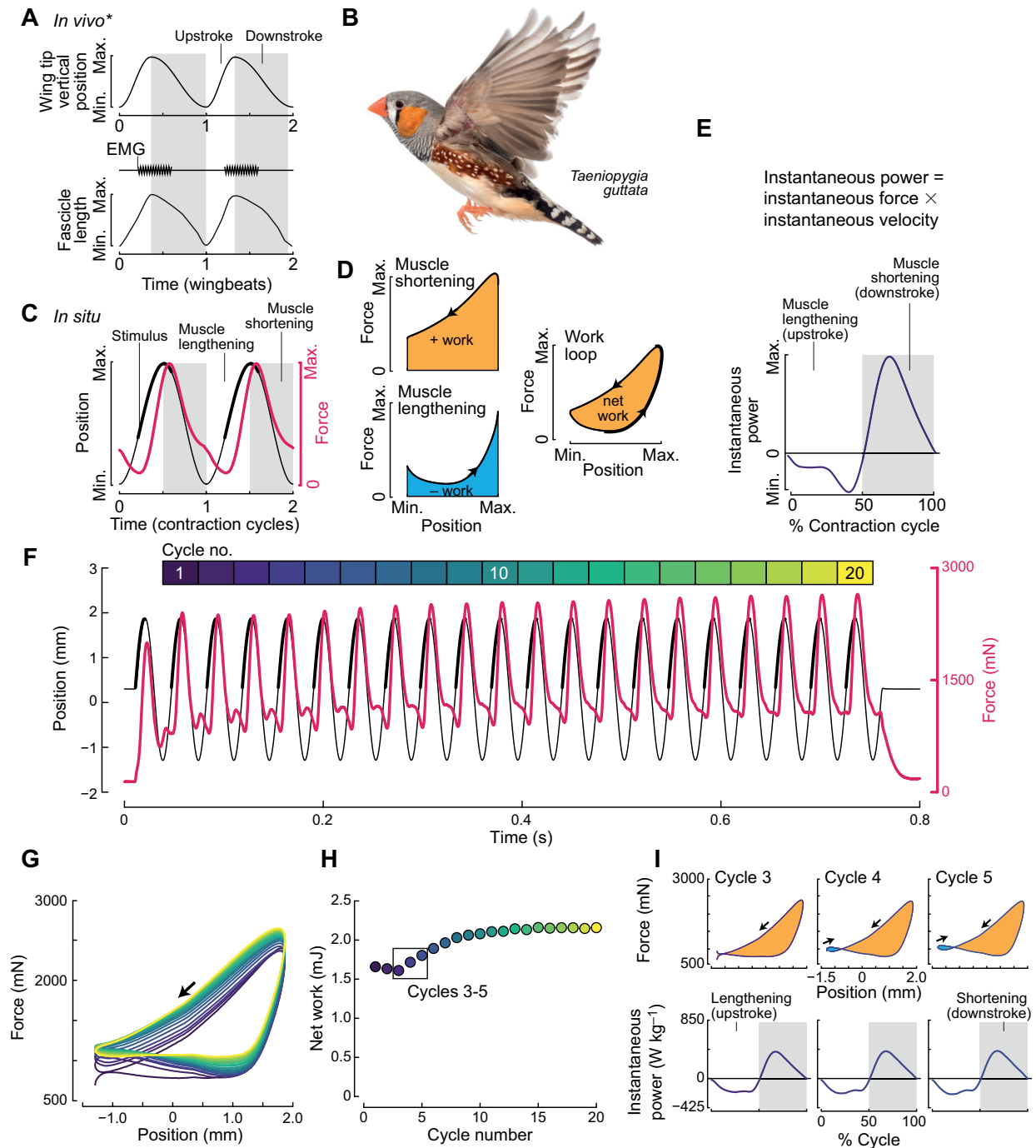


Fig. 1. Descriptive metrics of wing motion and muscle performance recorded *in vivo* used to establish the mean and range for each of the input parameters that define a contraction cycle in the *in situ* experiments. Instantaneous power and net power were calculated for each *in situ* trial and used to compare performance across trials. (A) Schematic illustrations of the metrics recorded from *in vivo* studies of zebra finches (*Taeniopygia guttata*; B) that inform the input parameters for this *in situ* muscle study. Although measured from different structures, the start and duration of the wing downstroke and upstroke correspond to the start and duration of pectoralis shortening and lengthening phases, respectively. *Traces in A are inspired by previous studies but do not display actual *in vivo* data. Image credit for B: GlobalP. (C) *In situ* trials involve attaching the muscle's insertion to a servo motor and implanting stimulating electrodes at opposite ends of the muscle. (D) Net work of a cycle is calculated by quantifying the positive work produced during the muscle's shortening phase and subtracting the negative work absorbed during the muscle's lengthening phase. (E) Plotting instantaneous power (the product of instantaneous force and instantaneous velocity) over a given cycle provides a profile of the rate of change of work performed by the muscle during the cycle. (F) An initial *in situ* recording from a zebra finch pectoralis major depicts raw position (black line) and force (red line) for 20 consecutive cycles. The settings for this trial were a cycle frequency of 28 Hz, a strain amplitude of 1.58 mm (~15% strain), a stimulus phase at -20% cycle phase, and a stimulus duration of 4 pulses at 300 Hz. Stimulus timing is indicated by thick black lines. Color bar (top) indicates cycle number. (G) Work loops from the 20 peak-to-peak cycles are plotted. (H) Net work is calculated as the area of the work loop. The box encloses cycles 3–5, which were used for all subsequent trials. (I) The work loop traces for cycles 3–5 are plotted above and the corresponding instantaneous power is plotted below.

The muscle was directly stimulated by running an electrical current between electrodes at opposite ends of the muscle: one on the anterior border of the muscle at the midpoint of the clavicle, and one at the posterior apex of the muscle. Each stimulating electrode was made of single stranded silver wire (0.1 mm diameter) insulated with polyimide (HML, California Fine Wire, Grover Beach, CA, USA) with 0.5 mm of insulation stripped from the end. Electrodes were inserted using a 30-gauge needle and secured with suture. Stimulation was provided by a high-power, bi-phase stimulator (model 701B, Aurora Scientific Inc.), which was operated under constant current following the time profile specific to each trial. The consequence was that the whole muscle was stimulated simultaneously and at the same fixed frequency, with a clearly defined onset and offset.

Work-loop parameter selection

For each preparation, we first determined the optimal stimulus parameters and the peak of the length–tension curve. Pulse frequency was selected by increasing the value until the maximum isometric tetanic force plateaued. The resulting frequency of 300 Hz was close to the value of 275 Hz used by Ellerby and Askew (2007a). Stimulus intensity was determined by increasing stimulus voltage and selecting the value where maximum isometric twitch force reached a plateau.

Resting length was determined by increasing the muscle attachment at the motor arm by 0.5 mm increments and recording a twitch. At each distance increment, the developed force was calculated as the difference between the passive tension (baseline) and peak force. The motor arm position and muscle resting length were chosen at the beginning of the plateau in a plot of force versus length that balanced maximum force production with low passive tension. The peak force length was defined as the length that produced the highest force over a series of isometric twitch contractions at increasing lengths. This enabled us to set the maximum excursion to occur at the peak force length for all subsequent work-loop trials because this matched observed *in vivo* patterns from zebra finches (Ellerby and Askew, 2007a).

Strain values were calculated as the change in muscle length along the medial axis of the muscle (a line from the humeral insertion to the midpoint of the muscle's inferior border), normalized by the mean postmortem resting length (measured using calipers after the bird was euthanized and the pectoralis was removed). For experiments, strain amplitude was defined as one half of the peak-to-trough distance of a cosine-wave strain trajectory. The full range of amplitudes (1.38–1.76 mm) represented approximately 13.1–16.8% of overall strain, given a mean muscle length of approximately 21 mm (Tables S1 and S2). These experiments were designed to cover a similar range of strains to those observed from *in vivo* fascicles (Ellerby and Askew, 2007b). The magnitudes and the range of strains were nearly identical between the *in vivo* and *in situ* condition for any fascicles oriented along the line of action (the length) of the muscle. However, because the muscle is multipennate, the *in situ* range of imposed strains varied for different fascicles depending on their exact orientation.

Work-loop experiments

Work-loop trials were programmed and controlled with proprietary software (Digital Muscle Controller, Aurora Scientific Inc.). We conducted work-loop trials by controlling length and recording force across a series of consecutive cycles. Muscle temperature was maintained at $40.0 \pm 0.2^\circ\text{C}$ with an incandescent lamp and recorded with a thermocouple probe (Bonner Scientific).

We initially tested 20 consecutive cycles to determine how many cycles are required to reach maximum work output. Peak force and work increased with each subsequent cycle and then approached a plateau after ~12 cycles (Fig. 1F–H). However, testing for 20

consecutive cycles caused the deeply anesthetized birds to die within minutes following the trial. We do not know the specific cause of death, but it is possible that this level of stimulation in combination with compression from the body brace overstressed the bird. Zebra finches naturally use a flap bounding behavior at all flight speeds, alternating a few consecutive wingbeats (3–9 depending on flight speed) with tucked wing bounding phases (Ellerby and Askew, 2007b; Tobalske et al., 1999). We therefore decided to perform all subsequent experiments with trials with five cycles and 90 s rest intervals. The result for each trial was the mean of the third to fifth cycle (Fig. 1H). This protocol allowed for dozens of trials over several hours without death or a substantial decrease in muscle power output. Although five cycles do not capture the absolute maximum performance of the muscle, using results from these trials only limits cumulative force development and provides a consistent comparison for all trials that is also better matched to the natural flapping behavior of the birds (Tobalske et al., 1999; Ellerby and Askew, 2007b).

Before investigating the effects of muscle strain amplitude and cycle frequency, we determined the stimulus parameters (duration and phase) that maximized muscle power output. We performed this test at an intermediate amplitude of 1.58 mm. For this phase of the study, we selected three muscle cycle frequencies (26, 28 and 30 Hz) that are close to the mean wingbeat frequency displayed by zebra finches during hovering and free flight (Ellerby and Askew, 2007b). We used short stimulus pulses of 0.2 ms delivered at 300 Hz. Stimulus duration is given as the period from the onset of the first pulse to the offset of the last. For example, a two-pulse stimulus train provided 3.53 ms of stimulus duration. We tested increasingly longer stimulus durations to determine the maximum net power, and then extended duration further to confirm that we had measured the peak value (Table S2).

We next tested a broad range of eight stimulus phase values at 28 Hz cycle frequency for each of three stimulus durations (24 iterations): (1) the duration that produced the highest power output, (2) a duration one pulse longer and (3) a duration one pulse shorter. Stimulus phase was defined as the time of stimulus onset relative to the time of peak length, and expressed as a percentage of cycle period. The sampled stimulus phase values ranged from the earliest value of -35% (12.5 ms of the cycle before peak length) to $+10\%$ (3.6 ms of the cycle after peak length).

Informed by the initial experiments on stimulus duration and phase, we designed eight experiments to determine how variation in strain amplitude and cycle frequency affect muscle power output (experiments 7–14 in Table S2). Because power output was maximized at a stimulus duration of either 3 or 4 pulses (6.86 and 10.19 ms) and a stimulus phase of either -30% or -20% , we used these specific parameters to make a 2×2 experimental design. The first experiment (-20% phase, 4 pulse duration) best approximates the *in vivo* activation duration and phase of zebra finches (-18% to -15% phase, 13–16 ms duration; Ellerby and Askew, 2007b). The other three experiments allow for comparison with an earlier phase, a shorter duration, or both. Within each of these four stimulus/phase combinations, we sampled a range of shortening velocities, first by varying only strain amplitude and then by varying only cycle frequency. The same range of mean muscle shortening velocity was tested in each case (154.3 – 197.6 mm s^{-1}), surrounding a mean shortening velocity of 175 mm s^{-1} .

Data analysis

Force and position were recorded at 10,000 Hz, and the difference between each time step was the duration over which instantaneous

velocity was calculated. Work and power calculated over these intervals is referred to hereafter as instantaneous work and power. Work calculated on a per cycle basis and then averaged over cycles three to five in each trial is referred to hereafter as the net work. The product of net work and the cycle frequency is the net power, and was normalized by muscle mass and presented in units of $W\text{ kg}^{-1}$. Data import and calculation of instantaneous work, instantaneous power, net work, net power, and muscle twitch kinetics were all performed via the R package *workloopR* (Baliga and Senthivasan, 2019).

To account for any degradation of the muscle over subsequent trials, the same parameters were used for the first and last trial in a sequence. The decline in power output was assumed to be a linear function of trial number, and all trials in a sequence were adjusted based on the difference between the first and last trial (Ellerby and Askew, 2007a; Fig. S1). A monitoring trial was taken between each treatment sequence, and this monitor was used to control for degradation in muscle output over several hours of data collection. Muscle power remained above 75% of maximum net power from the initial trial for all birds through all experiments, and remained above 90% in most cases.

We calculated peak isometric force by recording the peak tetanic force and dividing by physiological cross-sectional area (PCSA). PCSA was calculated as:

$$\text{PCSA} = \frac{\text{muscle mass}}{\text{muscle density} \times \text{fiber length}}, \quad (4)$$

using 1060 kg m^{-3} as muscle density. Fiber length is extremely variable in the pectoralis, and so we quantified fiber length as the mean between the short axis of the muscle (i.e. the shortest distance between the humeral attachment and the sternum) and the long axis of the muscle (i.e. distance between the humeral attachment and the caudal ends of the sternum). The pennation angle also varies along the length of the muscles, but should be approximately similar among individual zebra finches. For this reason, we opted for a definition of the PCSA that did not include pennation angle.

To determine the relative effects of cycle frequency and strain amplitude on muscle performance over a range of stimulus duration and phase values, we analyzed the results of these experiments in a linear mixed-model framework. The sampled data are portions of larger net power–velocity curves, but the sampled regions were small enough that linear approximations provided effective comparisons among treatments. Because it is possible that some factors interactively affect muscle performance or not at all, we compared six models that included different components (Table S3). As some individuals were used in multiple experiments, individual bird identity was used as a random effect in all models. Amplitude, frequency, stimulus duration (pulses) and/or stimulus phase were used as fixed effects. Fitted models were checked for power, overdispersion and singularity via the *performance* (<https://github.com/easystats/performance>) and *simr* (Green and MacLeod, 2016) software packages. Sample size was limited to four birds per experiment.

RESULTS

Quality assessment of the novel *in situ* preparation

We first asked whether our new work-loop preparation produces similar values to those measured previously from skinned fibers and fiber bundles. Specifically, we compared the isometric stress, defined as the peak tetanic force divided by PCSA, between our measurements of the whole muscle and measurements from muscle fibers (Ellerby and Askew, 2007a; Reiser et al., 2013). PCSA is challenging to accurately quantify for the avian pectoralis major because the muscle's

multi-pennate architecture and complex shape cause substantial variation in fiber length and pennation angle. Moreover, the muscle has a wide base with more than 45 deg variation in fiber orientation. The high pennation angles mean only a portion of the force of the individual fibers is in line with the muscle's central axis and the motor. We measured peak force during tetanus after the experiments for all birds that appeared to be physiologically stable. We decided to wait until after the experiments because we were concerned that tetanic stimulation would lead to significant muscle degradation. The one exception was bird 1, with which we measured tetanic force prior to the experiments. For that individual, force during tetanus was twice the value recorded for other birds (Table S1). The cause of this difference is unknown but could be related to the order of measurements.

Understanding these caveats, we calculated a peak isometric stress of $101 \pm 18\text{ kN m}^{-2}$, which is higher than estimates for individual skinned fibers from zebra finch pectoralis, $\sim 63\text{ kN m}^{-2}$ (Reiser et al., 2013), but lower than measurements for fiber bundles of the same species, $167 \pm 12\text{ kN m}^{-2}$ (Ellerby and Askew, 2007a). Thus, our whole-muscle work-loop preparation produces stress values that are similar to those from previous work with muscle fibers and fiber bundles.

Because extracellular stimulation can decrease the timing of force rise and relaxation (Sponberg et al., 2011), we also compared the timing of twitch kinetics against those from zebra finch fiber bundles (Ellerby and Askew, 2007a). Time to peak force for isometric twitches was $12.4 \pm 0.58\text{ ms}$ for our whole-muscle preparation, whereas measurements on zebra finch fiber bundles achieved peak force in $9.7 \pm 0.7\text{ ms}$. Thus, our direct muscle stimulation preparation led to a slight increase in the timing of force development, rather than a decrease. This may reflect the need for shorter stimulus durations in our whole-muscle work-loop rig to ensure that the muscle relaxes properly. Although we cannot make a direct comparison of *in situ* and *in vivo* force development timing, our whole-muscle preparation does not appear to decrease the timing of twitch kinetics compared with other-work loop studies of the same muscle. These effects may be related to the size of tissue stimulated or the use of isoflurane during our experiments (Kunst et al., 1999).

Effects of stimulus duration and phase on muscle power output

The stimulus duration that maximized net power output ranged from 6.86 to 10.19 ms depending on the cycle frequency and the individual. A stimulus duration of 6.86 ms (3 pulses) maximized power output at 30 Hz cycle frequency, whereas stimulus duration of 10.19 ms (4 pulses) maximized power output at 26 Hz (Fig. 2A). These stimulus durations are lower than *in vivo* activation durations (12–14 ms) recorded from the pectoralis major in zebra finches (Ellerby and Askew, 2007b). This difference may be explained by three differences between *in vivo* measurements and our *in situ* experiments, which used stimulus pulses of constant intensity and strain with equal shortening and lengthening phases on anesthetized birds. (1) The *in vivo* EMG pattern from freely flying zebra finches has varying activation intensity, like other multi-unit muscle recordings. (2) Strain during *in vivo* flight of this species is asymmetrical with a longer shortening than lengthening phase. (3) Prolonged relaxation has been observed in mammalian skeletal muscle while using isoflurane to anesthetize subjects (Kunst et al., 1999), but it is not clear whether this effect occurs in birds. Nonetheless, the stimulus durations that maximized power are relatively short, only about 12–18% of the time required to achieve tetanus ($\sim 60\text{ ms}$).

Understanding why longer stimulus duration led to such dramatic changes in net power output requires comparing the changes in

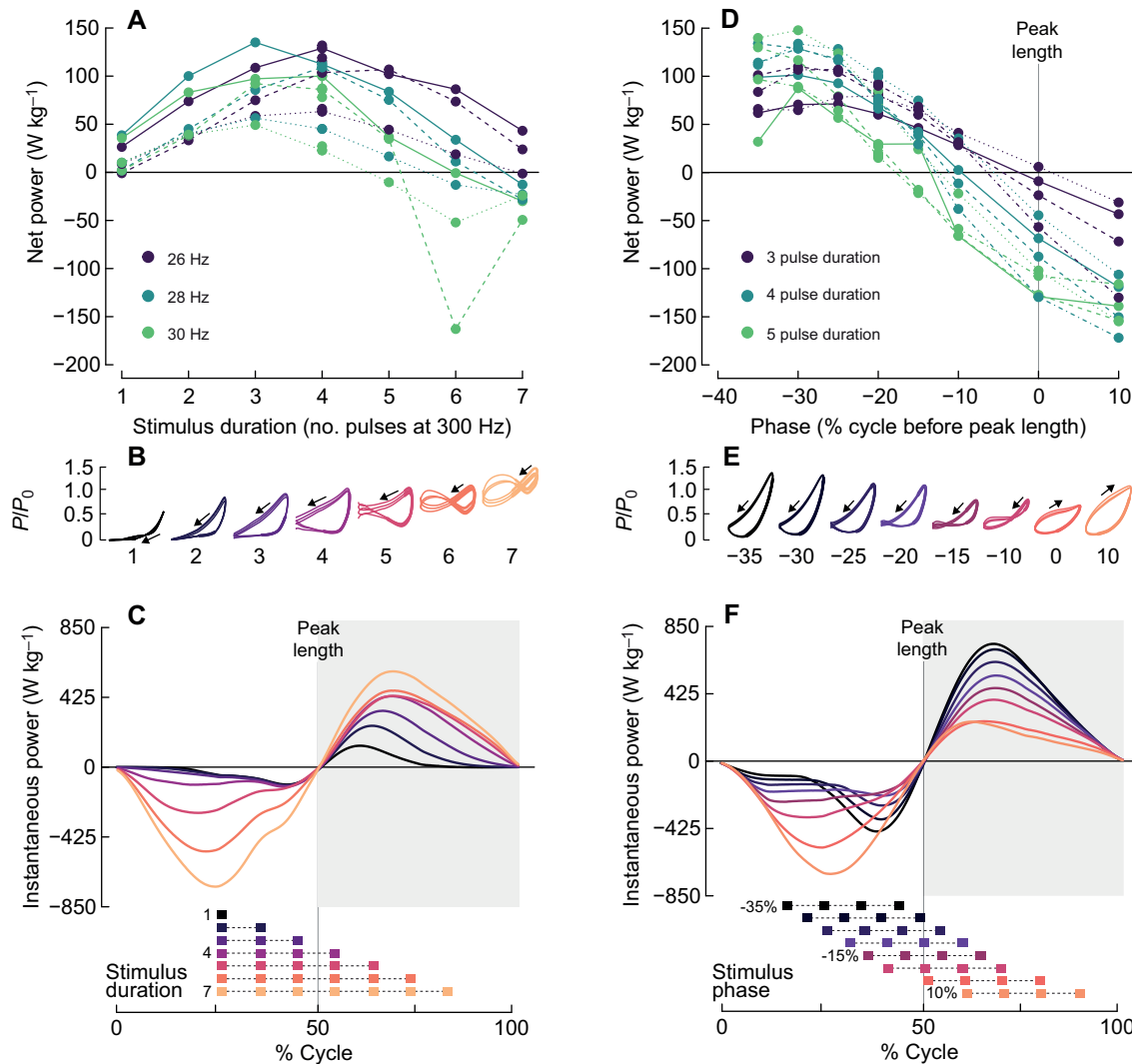


Fig. 2. Muscles cycling at high frequency generate substantial lengthening power. (A) Net muscle power is maximized at a stimulus duration of 3–4 pulses (experiments 1–3; Table S3). Data from three individuals are distinguished by line type, and color indicates cycle frequency. (B) Work loops from the solid teal line in A (one individual tested at 28 Hz) are plotted with the stimulus timing indicated by the thick line. P/P_0 , proportional stress. (C) The same trials are plotted as instantaneous power (product of instantaneous force and velocity), with color and colored bars at the bottom indicating stimulus duration and timing. (D) Net power is maximized at a stimulus phase close to –30% of the cycle before peak length (experiments 4–6; Table S3). Work loops (E) and instantaneous power (F) from the solid teal line in D [one individual tested at 4 pulse (10.19 ms) duration].

instantaneous performance within the work loop. Although changes in work-loop shape do illustrate the phenomena (Fig. 2B), comparing plots of instantaneous power versus time more clearly illustrates the difference between trials (Fig. 2C). During the first half of the cycle (0–50%), power production during muscle lengthening increases substantially with increases in stimulus duration above 10.19 ms (4 pulses). This is because the stimulus from the previous cycle produces force that persists into the lengthening phase. In contrast, during the second half of the cycle (50–100%), power production during shortening increases more modestly as a function of stimulus durations above 10.19 ms.

Increases in lengthening power caused by longer stimulus durations could be reduced by shifting stimulus phase earlier. The earlier stimulus phases (35% to 20% of the cycle prior to peak length) led to the highest net power (Fig. 2D), and the underlying cause is clear from plotting instantaneous power through the cycle (Fig. 2F): earlier phase led to low lengthening power and high shortening power. The phases that maximized net power (–30% to

–20%) were slightly earlier than the *in vivo* EMG phases (–18% to –15%) from zebra finches flying over a range of flight speeds (Ellerby and Askew, 2007b).

Effects of strain amplitude and cycle frequency on net power output

To understand how zebra finches could increase muscle shortening velocity given lengthening power constraints, we examined how increases in strain amplitude and cycle frequency affect muscle power output independently.

Across a range of strain amplitude, cycle frequency stimulus duration and stimulus phase that were inspired by the *in vivo* behavior of zebra finches, the best-fitting model showed that all four factors affect net power (Table S3; Fig. 3A). Cycle frequency also had important interactions with stimulus duration and stimulus phase. Although a model that included interactions between stimulus parameters and frequency along with interactions between stimulus parameters and amplitude provided nearly as good a fit to the data

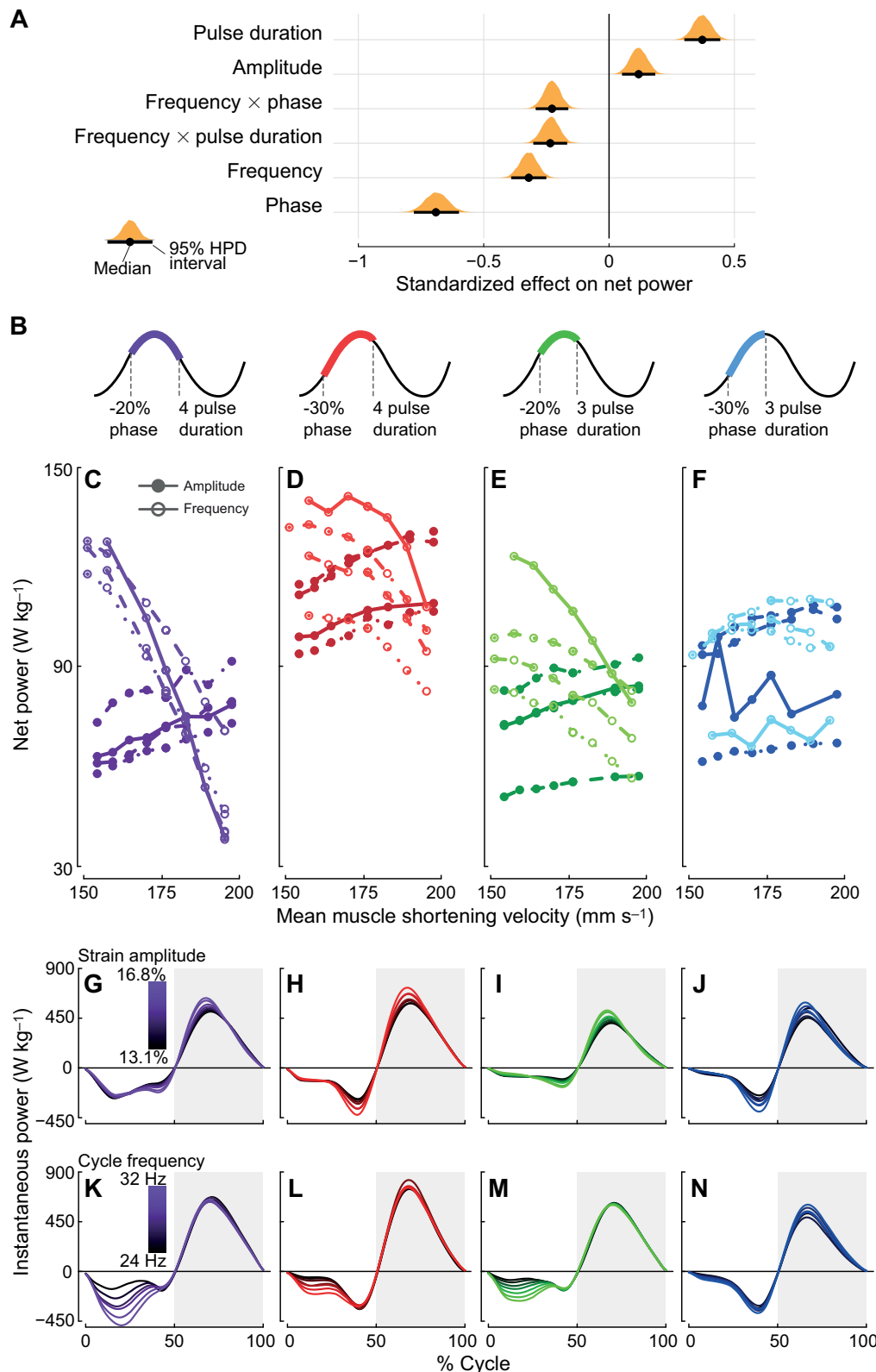


Fig. 3. Net power output increases with amplitude but decreases with frequency as a result of power production during the lengthening phase. (A) Standardized effects of all fixed effects from the best-fitting mixed model (Table S3) that explained variation in net power. Larger absolute values indicate stronger effects on net power. Dots indicate medians of posterior distributions, thick black lines depict 95% highest posterior density (HPD) intervals, and orange shading shows the distribution of posterior samples. (B) Phase (relative to peak length) and stimulus duration (pulses) for each of the key experiments, shown graphically on a sine wave. (C–F) Net power, which is the average of instantaneous power for a cycle, plotted against mean muscle shortening velocity, which is calculated from each trial's displacement amplitude and cycle frequency. The slopes of the net power curves for amplitude are similar across stimulus treatments because the increases in negative and positive power are similar across all treatments. In contrast, the slopes of net power curves for frequency differ across treatments because of the large variation in lengthening power. (G–N) The instantaneous power plots depict one individual (solid line) from each of the matched plots (bottom row).

(Δ deviance information criteria, ΔDIC 2.79), the effects of interactions between stimulus parameters and amplitude were weak and could not sufficiently be distinguished from zero (95% highest posterior density, HPD: -0.064 to 0.093 and -0.050 to 0.106). Overall, models containing all of cycle frequency, strain amplitude, stimulus duration and stimulus phase performed substantially better

than an intercept-only model. Similar results were found when duty cycle was used in place of stimulus duration (Table S4).

Delaying stimulus phase and increasing cycle frequency strongly and negatively affected net power output (Fig. 3A). Delaying stimulus phase also made the effect that increasing frequency had on net power more negative. Similarly, increasing stimulus duration

caused the effect of frequency on net power to trend more negatively. In contrast, increasing stimulus duration and strain amplitude both led to higher net power. Whereas the direction of effects of stimulus phase and duration are expected based on the initial experiments and indeed on decades of muscle physiology research (Josephson, 1985; Dickinson et al., 2000; Syme, 2005), the contrasting effects of cycle frequency and strain amplitude are unusual.

The distinctions between the effect of amplitude and frequency confirm our initial prediction that increasing muscle strain amplitude from the baseline produces more muscle power output than increasing frequency. The 95% HPD intervals of these effects each exclude zero and are also distinct from each other (amplitude 95% HPD: 0.054–0.185; frequency 95% HPD: –0.390 to –0.254; Table S3).

The diverging consequences of changing amplitude and frequency can be visualized by plotting net power against mean muscle shortening velocity (Fig. 3C–F). The slope of the relationship when due to changes in strain amplitude was positive and was similar for all four experiments. In contrast, increasing cycle frequency generally led to declines in net power, but the slopes depended on interactions with both stimulus phase and duration. For the experiment that was most similar to *in vivo* conditions (–20% phase, 4 pulses) (Ellerby and Askew, 2007b), increasing frequency led to the sharpest decline in net power (Fig. 3C). For the next experiment, in which stimulus phase was advanced but for the same stimulus duration, the decline in muscle power with increased frequency was muted. Net power remained relatively high even as cycle frequency increased (Fig. 3D). In contrast, shorter stimulus durations of only 3 pulses led to lower power overall (Fig. 3E,F). However, the combination of advanced phase and short duration (–30% phase, 3 pulses) produced a positive relationship between net power and increases in velocity via cycle frequency (Fig. 3F). Collectively, these experiments demonstrate that the effects of manipulating frequency to modulate muscle shortening velocity are interactively affected by stimulation parameters, but the manipulation of amplitude is relatively unaffected by stimulation regime.

Plots of the treatment-specific work loops reinforce the finding that strain amplitude and cycle frequency can have opposing effects on muscle output, depending on the stimulation (Fig. 4A,B). In experiments with late stimulus phase and longer duration, work loops expanded as frequency was decreased and compressed as frequency was increased (Fig. 4A). Experiments with an early stimulus phase and shorter duration showed the opposite trend: work loops showed slight compression as frequency decreased and expansion as frequency increased (Fig. 4B). Increasing amplitude, by definition, increases the width of a work loop, but higher amplitudes also tended to produce increases in maximum force during shortening.

Although informative, changes in work-loop shape tend to reveal more about changes to net work rather than to net power. How variation in strain amplitude and cycle frequency lead to opposing effects on net power can be viewed in plots of instantaneous power. Fig. 3G–N provides the average instantaneous power results for one representative bird from each experiment. Similar trends held for the first three experiments. Increasing wingbeat frequency led to greater lengthening power, with little to no change in shortening power (Fig. 3K–M). In contrast, increasing strain amplitude led to only modest changes in lengthening power, which were outweighed by increases in shortening power (Fig. 3G–I). The exception to these trends came from the experiment with advanced phase (–30%) and short stimulus duration (3 pulses). Here, modest increases in lengthening power were countered by slightly greater increases in shortening power for both amplitude and frequency manipulations (Fig. 3J,N).

DISCUSSION

To determine how increasing muscle shortening velocity affects the performance of a high-frequency muscle, we developed a novel *in situ* muscle work-loop rig (Fig. 1) to measure instantaneous force from the pectoralis major of zebra finches (mean wingbeat frequency 26 Hz). This approach allowed for several experiments from each individual bird (Fig. S1), and collectively permitted us to test the effects of stimulus duration, phase, cycle frequency and strain amplitude for the range of values observed *in vivo* (Ellerby and Askew, 2007b). At the stimulus duration and stimulus phase that produced maximum power output, the instantaneous force and power produced during muscle lengthening was substantial (Fig. 2). This result suggests a hypothesis for why zebra finches *in vivo* modulated wing stroke amplitude more than wingbeat frequency (Ellerby and Askew, 2007b): these two kinematic mechanisms for changing muscle shortening velocity differ with respect to the ratio of shortening to lengthening power. We tested this hypothesis by directly comparing changes in shortening velocity due to changing either strain amplitude or cycle frequency (Fig. 3). The experimental values used for shortening velocity, strain amplitude and cycle frequency were designed to cover a similar range to the *in vivo* values over which zebra finches exhibited increased wingbeat amplitude over wingbeat frequency. Whereas increases in cycle frequency often lead to dramatic increases in lengthening power and thus decreased net power output, increases in strain amplitude consistently produced higher muscle power output. Collectively, these experiments suggest that birds using high wingbeat frequency, such as zebra finches, should favor increases in wing stroke amplitude over further increases in wingbeat frequency to meet more demanding aerodynamic challenges.

Hummingbirds, which use the highest wingbeat frequencies of any bird (Greenewalt, 1962; Altshuler and Dudley, 2003; Donovan et al., 2013), tend to modulate stroke amplitude over wingbeat frequency, especially during sustained performance. During many challenges, including sub-maximum load lifting (Mahalingam and Welch, 2013), increasing flight speed (Tobalske et al., 2007) and flying in reduced air density (Altshuler et al., 2010b; Chai and Dudley, 1995, 1996; Chai et al., 1997), the main observed change is in stroke amplitude rather than wingbeat frequency. The only times when hummingbirds have been observed to generate substantial increases of wingbeat frequency are during brief courtship displays (Clark et al., 2013) and maximum load lifting (Chai et al., 1997; Chai and Millard, 1997; Altshuler and Dudley, 2003).

Although the results of our experiments provide a potential explanation for the observed wingbeat kinematics of small birds, there are several important caveats for interpreting *in situ* muscle results relative to *in vivo* activity. *In vivo* muscle activation occurs through the recruitment of motor units at different locations and with different temporal patterns of activation. In contrast, muscle stimulation *in situ* occurs by simultaneous current injection to the entire muscle and with the same fixed frequency. This general constraint of muscle stimulus studies will affect how work, including lengthening work, is generated from each motor unit. A specific constraint of our *in situ* stimulus is that the phase was always defined as a percentage of the cycle, and the duration was always defined in milliseconds. This means that as frequency was increased, the absolute time (in ms) before peak strain became lower for phase onset, and the stimulus duty cycle (in % cycle) became longer. In contrast, for the amplitude manipulations, the onset phase and stimulus duty cycle remained constant, both in terms of percentage of cycle and in absolute time.

How does the variation caused by this experimental design compare with the *in vivo* data? Ellerby and Askew (2007a) tested a

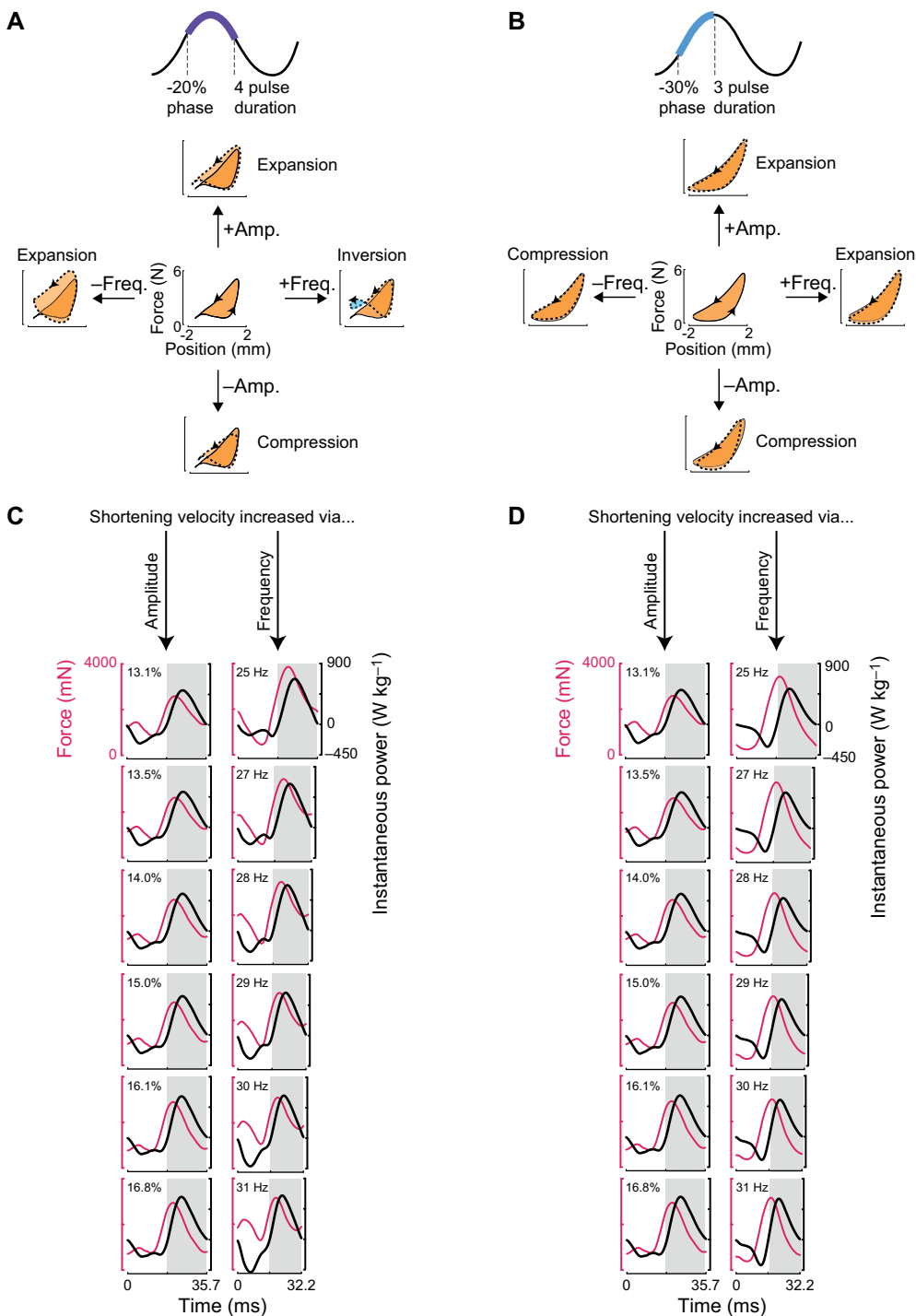


Fig. 4. Expansion of results for experiments 7–14. (A,B) Strain amplitude and cycle frequency had opposing effects on muscle work, which also depend on stimulus pattern. In experiments with late stimulus phase and longer duration, work loops expanded as frequency was decreased and compressed as frequency was increased (A). In contrast, work loops showed slight compression and expansion as frequency increased in experiments with early stimulus phase and shorter duration (B). Increasing amplitude generally resulted in expansion (principally in width) of work loops regardless of stimulus pattern (both A and B). (C,D) Visualizing the time course of both force and instantaneous power for the experimental conditions in A and B, respectively, illustrates that during muscle lengthening (white), increases in cycle frequency lead to higher forces and power. In contrast, increases in strain amplitude have smaller effects on force and power during muscle lengthening.

range of stimulus onsets in their *in vitro* preparation that best matched their *in vivo* study (Ellerby and Askew, 2007b). These stimulus onsets varied by up to 0.7 ms. Within each of our four frequency treatments at the extremes, stimulus onset varied by a maximum of 2 ms in the case of the -20% phase onset and by 3 ms in the case of the -30% phase onset. The purpose of our experiments was to test specifically over a broad range, but it is worth noting that the middle four treatments within each experiment varied by a similar level of only 0.7 ms. Our duty cycle varied by a maximum of $\sim 5.5\%$ for the 3-pulse stimulus and by $\sim 8\%$ for the 4-pulse stimulus. These values can be more directly compared with the *in vivo* data (Ellerby and Askew, 2007b; see their fig.3 A), and are within the same level of

variation as the standard errors of the mean values. Zebra finches exhibit relatively high variation in EMG duty cycles, which when combined with relatively modest changes in wingbeat frequency, can explain why neither activation duration nor duty cycle changed significantly across flight speeds (Ellerby and Askew, 2007b). Overall, this comparison suggests that although our experiments expanded the envelope of stimulus onset and duration to some degree when compared with *in vivo* data, the experiments are largely comparable with muscle activity in flight.

We were able to quantify the effect of duty cycle on net power by reanalyzing our entire dataset (Table S4), which included a range of duty cycle from 0.01 to 0.64. In Fig. 5, we plot the relationship

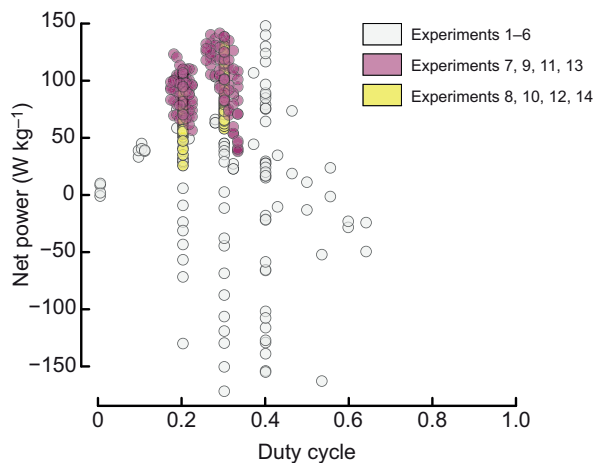


Fig. 5. Relationship between net power and duty cycle for the entire dataset (all trials across all experiments and all individuals). Peak net power was found at the intermediate values for duty cycle that were investigated. All duty cycles from the amplitude/frequency experiments (experiments 7–14) fell near the peak of positive power.

between net power and duty cycle. The highest net power values were located at the intermediate values for duty cycle that were tested. Most importantly, all of the duty cycles used in the amplitude/frequency experiments in Fig. 3 resulted in net power values that were among the highest of all experiments. The plateau in net power values indicates that variation in stimulus duty cycle due to the frequency manipulation was modest with respect to muscle performance.

Another important axis of variation for muscle activity is the strain trajectory. Zebra finches, and many other avian species, have shortening durations that are typically longer than lengthening durations (Biewener et al., 1998; Williamson et al., 2001; Hedrick et al., 2003; Ellerby and Askew, 2007b; Tobalske et al., 2010; Robertson and Biewener, 2012). In contrast, our work-loop experiments used only sinusoidal length changes. The amplitude/frequency experiments that were closest to *in vivo* conditions had -20% phase and 4 pulse duration (Table S2, experiments 13 and 14). For shortening velocities less than 175 mm s^{-1} (Fig. 3C), increases in wingbeat frequency led to reduced net power, but still generated higher net power than increases via strain amplitude. This result leads to the question of why zebra finches *in vivo* would ever use wingbeat frequencies above that crossover value for shortening velocity. One possibility is that wingbeat frequencies of $\sim 25\text{--}30 \text{ Hz}$ do not produce as much wasteful power as our measurements suggest because zebra finches' natural strain trajectories allow more time for the pectoralis muscle to relax. For example, the benefits of a longer shortening phase for cyclic contractions have been demonstrated for the mouse extensor digitorum longus and soleus muscles operating at 5 and 11 Hz, respectively. Askew and Marsh (1997) made *in situ* work-loop measurements and directly compared sinusoidal with saw tooth strain and were able to examine saw tooth strains that had longer shortening or lengthening phases. For both mouse muscles, strain cycles with longer shortening phases produced the largest net power. Thus, although the overall trends for how changes in strain amplitude and cycle frequency affect net power in the zebra finch pectoralis major are consistent, the slopes and crossover point may shift in future experiments that probe the effects of asymmetrical shortening/lengthening strain.

Given the deleterious effects of increasing muscle shortening velocity via cycle frequency, why would any bird that has a high

baseline wingbeat frequency choose to increase this kinematic feature to meet an aerodynamic challenge? One answer is that longer activation durations may confer benefits by generating a more powerful shortening phase during the downstroke. Some of the trials with high negative power during lengthening produced even higher positive power during shortening phase (Figs 3 and 4), though net power over the entire cycle was lower. If the animal is not optimizing energetic efficiency, it can use longer activation durations to produce more positive power during shortening and counter the extra negative power by increasing output of the antagonist muscle (the supracoracoideus). It is possible that small birds take advantage of this feature during behaviors that require a more powerful downstroke, such as load lifting and burst performance. Hummingbirds exhibit increased supracoracoideus activity during sub-maximal weight lifting (Mahalingam and Welch, 2013) and pigeons show increased supracoracoideus power output during ascending flight, even though their upstroke motion should contribute little to lift generation during ascending flight (Tobalske and Biewener, 2008). Moreover, hummingbirds increased the activation duration of their pectoralis major by a factor of three during load lifting (Altshuler et al., 2010a), which should cause pectoralis force production to persist into the lengthening phase.

It is not known whether longer muscle activation and increased wingbeat frequency lead to a decline in the mechanical efficiency of avian flight because answering this question would require simultaneous recoding of muscle activation, wing motion and metabolic rate. The only study that examined oxygen consumption under varying wingbeat kinematics in birds was a manipulation of air density during hovering in hummingbirds (Chai and Dudley, 1995). As air density increased, hummingbirds increased wingbeat frequency modestly and stroke amplitude considerably, which was accompanied by an increase in oxygen consumption and a concomitant decrease in muscle efficiency. Other studies of maximal load lifting in hummingbirds demonstrate strong changes in both stroke amplitude and wingbeat frequency (Chai et al., 1997; Chai and Millard, 1997; Altshuler and Dudley, 2003), leading to very high mechanical power output, but the efficiency is unknown for this behavior because there have been no metabolic measurements. To our knowledge, the only dataset that can directly evaluate how variation in wing stroke amplitude and wingbeat frequency affects efficiency is a study of fruit flies *Drosophila melanogaster*. The experiment involved tethering flies in a virtual reality environment along with simultaneous metabolic measurement (Lehmann and Dickinson, 1997). Visual stimuli caused flies to use a broad range of wingbeat frequency and wing stroke amplitude, which led to changes in wingbeat kinematics, sometimes with very low mechanical efficiency. The flies achieved maximum efficiency using submaximal wingbeat frequency but maximum wing stroke amplitude.

We next considered whether birds can increase wingbeat frequency in concert with net power by shortening activation duration. EMG measurements from hummingbird pectoral muscles have been recorded during hovering in low-density air, sub-maximum load lifting and maximum load lifting (Altshuler et al., 2010a; Mahalingam and Welch, 2013). The activation duration of the hummingbird EMG is extremely short, typically only one or a few spikes of synchronized motor unit activity lasting 1–2 ms (Hagiwara et al., 1968; Altshuler et al., 2010b; Tobalske et al., 2010). When challenged to hover in progressively less-dense air, hummingbirds primarily use changes in wing stroke amplitude to maintain aerodynamic force, with accompanying increases in EMG activation intensity (Altshuler et al., 2010b). The number of spikes in a hummingbird EMG (and therefore the activation duration) does not vary with either air density

(Altshuler et al., 2010b) or sub-maximum load (Mahalingam and Welch, 2013). The one treatment that caused hummingbirds to substantially increase wingbeat frequency is maximum load lifting, but this is also the only treatment that caused hummingbirds to increase their activation duration (Altshuler et al., 2010b). Thus, there is no evidence that hummingbirds decrease pectoral muscle activation duration to increase muscle power with increasing frequency. Evolutionary comparisons are also limited but it is possible that the extremely short activation during routine hovering flight of hummingbirds represents an adaptation to decrease antagonist muscle forces and increase mechanical power output.

A second option for mitigating the effect of high-frequency flapping on negative power production would be to shift the activation phase earlier. Both hummingbird and zebra finch pectoral muscles have an earlier activation phase compared with that of birds using lower wingbeat frequencies such as budgerigars and pigeons (Ellerby and Askew, 2007a; Tobalske et al., 2010). Muscle activation in both hummingbirds and zebra finches has been measured across a range of speeds in wind tunnels. For the hummingbirds, neither wingbeat frequency nor activation onset in the pectoralis major varied significantly with flight speed, but the onset of the antagonist muscle, the supracoracoideus, was more delayed at intermediate flight speeds (Tobalske et al., 2007, 2010). Zebra finches, in contrast, increased wingbeat frequency across flight speeds with concomitant advances in EMG onset for the pectoralis major (Ellerby and Askew, 2007a). Thus, there is some evidence for variation in activation onset in both species, and for the zebra finches, the data are consistent with the prediction that earlier onsets can be used to compensate for contraction at faster wingbeat frequencies.

Overall, our experiments reveal that for the activation parameters of birds using high wingbeat frequency, it is more beneficial to increase aerodynamic force by increasing wing velocity via wing stroke amplitude than via wingbeat frequency. However, consideration of the lift equation reveals that flapping birds can also modulate aerodynamic force through changes in air density, wing area and the lift coefficient, which varies with wing presentation such as camber (Altshuler et al., 2015). Some of these mechanisms may not be apparent from measurements of wingbeat or even muscle kinematics. For example, cockatiels (Hedrick et al., 2003) and hummingbirds (Tobalske et al., 2010) maintain similar strain amplitude and cycle

frequency across flight speeds but nonetheless exhibit changes in the spatial recruitment of motor units within muscles. Of the terms in the force equations, velocity has the greatest influence because it is raised to the second power. Thus, although birds can modulate force through wing morphing, at a given flight speed, modulation of wing stroke amplitude is likely to be the single most important avenue for adjusting aerodynamic force in small birds.

Across the full range of shortening velocity, muscle power exhibits an inverted U-shaped curve: intermediate velocity produces the highest net power (Fig. 6A,B). The complete power–velocity curve can be generated by varying velocity either only through amplitude (Syme and Stevens, 1989) or only through frequency (Josephson, 1993; Stevenson and Josephson, 1990). Although we did not measure muscle power across the full range of shortening velocities, the regions that we did measure (Fig. 3C–F) must necessarily be part of curves that have different shapes depending on the activation parameters (Fig. 6C,D). The shapes of the available portions of the curve suggest that at high cycle frequencies, small changes to activation phase and direction have strong effects on the location of the peak of the power–velocity curve. The closest matches to *in vivo* muscle activity in zebra finches are the curves with -20% phase and 4 pulse duration (Fig. 6C,D, purple), which suggests an especially prominent trade-off between modulation via amplitude and frequency. Moreover, the muscle shortening velocities of zebra finches are at the intermediate values that we tested and are therefore close to the crossover point between the amplitude and frequency curves. If other small birds using high wingbeat frequencies exist in a similar muscle activation regime, then this result may explain a general preference for amplitude over frequency. However, the other curves in Fig. 6C,D suggest that if a bird is able to use earlier onsets (red, blue) or similar onsets but with shorter durations (green), then they can operate in a different regime in which the tradeoff between amplitude and velocity is either absent or less extreme. The capacity to use a different power–velocity curve or to exist in a different region of a given power–velocity curve should be dictated by some combination of wing loading, muscle fiber composition and flight style.

Small birds that use high wingbeat frequencies are highly maneuverable, and multiple metrics of maneuverability are strongly associated with muscle capacity (Segre et al., 2015; Dakin et al.,

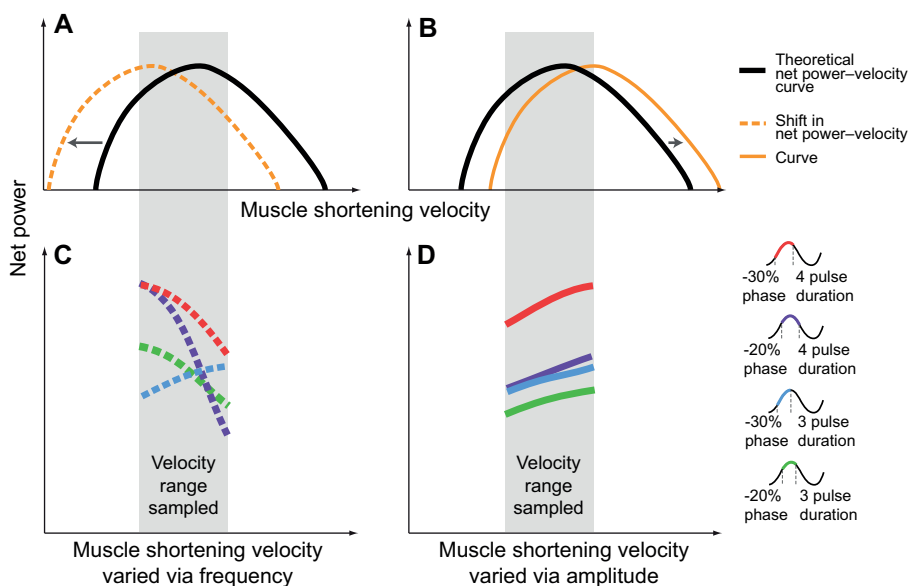


Fig. 6. Across the range of possible shortening velocity, a muscle will exhibit a power–velocity curve with an intermediate maximum. (A,B) The measurements from experiments 7–14 were made over the same range of shortening velocity (shaded region). (C,D) The resulting power–velocity relationships must necessarily be part of a larger power–velocity curve. For increases of shortening velocity through strain amplitude, differences among activation conditions did not cause major changes in the slope of the power–velocity relationships, but for a given stimulus duration, advancing the phase led to higher net power. In contrast, for increases in cycle frequency, small changes to activation phase and duration have substantial effects on the slope and magnitude of the power–velocity curves, and thus on the locations of peak power.

2018). This suggests that the ability to increase muscle shortening velocity via strain amplitude and cycle frequency confers advantages to catching prey, escaping predators and other essential behaviors. The challenge with increasing shortening velocity through increased wingbeat frequency is that high-frequency muscle oscillation leads to low force and power, and low efficiency (Syme and Josephson, 2002). Work-loop analysis of the avian pectoralis major reinforces this result for frequency but reveal the benefits of an alternative strategy for increasing muscle shortening velocity through strain amplitude. The inferior performance of increasing frequency results from increased negative power produced during the lengthening phase, i.e. upstroke. Our data show that for zebra finches, as the upper limits of flapping frequency are approached, a gradual reduction in the effectiveness of increasing frequency is observed. This biomechanical pattern should provide an opportunity to examine the relative contributions of wing stroke amplitude and wingbeat frequency to avian maneuverability.

Acknowledgements

This research began as a collaboration with Robert K. Josephson and the manuscript is dedicated to his memory.

Competing interests

The authors declare no competing or financial interests.

Author contributions

Conceptualization: J.W.B., D.L.A.; Methodology: J.W.B.; Software: V.B.B.; Validation: V.B.B.; Formal analysis: V.B.B.; Investigation: J.W.B.; Data curation: V.B.B.; Writing - original draft: J.W.B., V.B.B., D.L.A.; Writing - review & editing: J.W.B., V.B.B., D.L.A.; Visualization: J.W.B., V.B.B.; Supervision: D.L.A.; Project administration: D.L.A.; Funding acquisition: D.L.A.

Funding

J.W.B. was supported by a postdoctoral research fellowship from the National Science Foundation. The research was funded by grants from the Natural Sciences and Engineering Research Council of Canada (RGPIN-2016-05381), and the U.S. Air Force Office of Scientific Research (grant number FA9550-16-1-0182, monitored by Dr B. L. Lee).

Data availability

The original recordings of muscle strain, force and the stimulus timing parameters, as well as all analysis scripts and diagrams for immobilizing brace are available from figshare: <https://doi.org/10.6084/m9.figshare.12520733>

Supplementary information

Supplementary information available online at <https://jeb.biologists.org/lookup/doi/10.1242/jeb.225839.supplemental>

References

- Ahn, A. N. (2012). How muscles function - the work loop technique. *J. Exp. Biol.* **215**, 1051-1052. doi:10.1242/jeb.062752
- Altshuler, D. L. and Dudley, R. (2003). Kinematics of hovering hummingbird flight along simulated and natural elevational gradients. *J. Exp. Biol.* **206**, 3139-3147. doi:10.1242/jeb.00540
- Altshuler, D. L., Dudley, R., Heredia, S. M. and McGuire, J. A. (2010a). Allometry of hummingbird lifting performance. *J. Exp. Biol.* **213**, 725-734. doi:10.1242/jeb.037002
- Altshuler, D. L., Welch, K. C., Cho, B. H., Welch, D. B., Lin, A. F., Dickson, W. B. and Dickinson, M. H. (2010b). Neuromuscular control of wingbeat kinematics in Anna's hummingbirds (*Calypte anna*). *J. Exp. Biol.* **213**, 2507-2514. doi:10.1242/jeb.043497
- Altshuler, D. L., Bahlman, J. W., Dakin, R., Gaede, A. H., Goller, B., Lentink, D., Segre, P. S. and Skandalis, D. A. (2015). The biophysics of bird flight: functional relationships integrate aerodynamics, morphology, kinematics, muscles, and sensors. *Can. J. Zool.* **93**, 961-975. doi:10.1139/cjz-2015-0103
- Askew, G. N. and Marsh, R. L. (1997). The effects of length trajectory on the mechanical power output of mouse skeletal muscles. *J. Exp. Biol.* **200**, 3119-3131.
- Askew, G. N. and Marsh, R. L. (1998). Optimal shortening velocity ($V/V(\max)$) of skeletal muscle during cyclical contractions: Length-force effects and velocity-dependent activation and deactivation. *J. Exp. Biol.* **201**, 1527-1540.
- Askew, G. N. and Marsh, R. L. (2001). The mechanical power output of the pectoralis muscle of blue-breasted quail (*Coturnix chinensis*): The in vivo length cycle and its implications for muscle performance. *J. Exp. Biol.* **204**, 3587-3600.
- Bahlman, J. W., Swartz, S. M. and Breuer, K. S. (2014). How wing kinematics affect power requirements and aerodynamic force production in a robotic bat wing. *Bioinspir. Biomim.* **9**, 025008. doi:10.1088/1748-3182/9/2/025008
- Baliga, V. and Senthivasan, S. (2019). workloopR: Analysis of work loops and other data from muscle physiology experiments in R. *J. Open Source Softw.* **4**, 1856. doi:10.21105/joss.01856
- Biewener, A. A., Corning, W. R. and Tobalske, B. W. (1998). In vivo pectoralis muscle force-length behavior during level flight in pigeons (*Columba livia*). *J. Exp. Biol.* **201**, 3293-3307.
- Chai, P. and Dudley, R. (1995). Limits to vertebrate locomotor energetics suggested by hummingbirds hovering in heliox. *Nature* **377**, 722-725. doi:10.1038/377722a0
- Chai, P. and Dudley, R. (1996). Limits to flight energetics of hummingbirds hovering in hypodense and hypoxic gas mixtures. *J. Exp. Biol.* **199**, 2285-2295.
- Chai, P. and Millard, D. (1997). Flight and size constraints: Hovering performance of large hummingbirds under maximal loading. *J. Exp. Biol.* **200**, 2757-2763.
- Chai, P., Chen, J. S. C. and Dudley, R. (1997). Transient hovering performance of hummingbirds under conditions of maximal loading. *J. Exp. Biol.* **200**, 921-929.
- Clark, C. J., Feo, T. J. and van Dongen, W. F. D. (2013). Sounds and courtship displays of the peruvian sheartail, chilean woodstar, oasis hummingbird, and a hybrid male peruvian sheartail×chilean woodstar. *Condor* **115**, 558-575. doi:10.1525/cond.2013.120047
- Dakin, R., Segre, P. S., Straw, A. D. and Altshuler, D. L. (2018). Morphology, muscle capacity, skill, and maneuvering ability in hummingbirds. *Science (80-)* **657**, 653-657. doi:10.1126/science.120047
- Dickinson, M. H., Farley, C. T., Full, R. J., Koehl, M. A. R., Kram, R. and Lehman, S. (2000). How animals move: an integrative view. *Science (80-)* **288**, 100-106. doi:10.1126/science.288.5463.100
- Donovan, E. R., Keeney, B. K., Kung, E., Makan, S., Wild, J. M. and Altshuler, D. L. (2013). Muscle activation patterns and motor anatomy of Anna's hummingbirds *Calypte anna* and zebra finches *Taeniopygia guttata*. *Physiol. Biochem. Zool.* **86**, 27-46. doi:10.1086/668697
- Ellerby, D. J. and Askew, G. N. (2007a). Modulation of flight muscle power output in budgerigars *Melopsittacus undulatus* and zebra finches *Taeniopygia guttata*: in vitro muscle performance. *J. Exp. Biol.* **210**, 3780-3788. doi:10.1242/jeb.006288
- Ellerby, D. J. and Askew, G. N. (2007b). Modulation of pectoralis muscle function in budgerigars *Melopsittacus undulatus* and zebra finches *Taeniopygia guttata* in response to changing flight speed. *J. Exp. Biol.* **210**, 3789-3797. doi:10.1242/jeb.006296
- Green, P. and Macleod, C. J. (2016). SIMR: an R package for power analysis of generalized linear mixed models by simulation. *Methods Ecol. Evol.* **7**, 493-498. doi:10.1111/2041-210X.12504
- Greenewalt, C. H. (1962). Dimensional relationships for flying animals. *Smithson. Misc. Collect.* **144**, 243-266.
- Hagiwara, S., Chichibu, S. and Simpson, N. (1968). Neuromuscular mechanisms of wing beat in hummingbirds. *Z. Vgl. Physiol.* **60**, 209-218. doi:10.1007/BF00878451
- Hedrick, T. L., Tobalske, B. W. and Biewener, A. A. (2003). How cockatiels (*Nymphicus hollandicus*) modulate pectoralis power output across flight speeds. *J. Exp. Biol.* **206**, 1363-1378. doi:10.1242/jeb.00272
- Jackson, B. E. and Dial, K. P. (2011). Scaling of mechanical power output during burst escape flight in the Corvidae. *J. Exp. Biol.* **214**, 452-461. doi:10.1242/jeb.046789
- Josephson, R. K. (1985). Mechanical power output from striated muscle during cyclic contraction. *J. Exp. Biol.* **114**, 493-512.
- Josephson, R. K. (1993). Contraction dynamics and power output of skeletal muscle. *Annu. Rev. Physiol.* **55**, 527-546. doi:10.1146/annurev.ph.55.030193.002523
- Kunst, G., Graf, B. M., Schreiner, R., Martin, E. and Fink, R. H. A. (1999). Differential effects of sevoflurane, isoflurane, and halothane on Ca²⁺ release from the sarcoplasmic reticulum of skeletal muscle. *Anesthesiology* **91**, 179-186. doi:10.1097/0000542-199907000-00026
- Lehmann, F. O. and Dickinson, M. H. (1997). The changes in power requirements and muscle efficiency during elevated force production in the fruit fly *Drosophila melanogaster*. *J. Exp. Biol.* **200**, 1133-1143.
- Mahalingam, S. and Welch, K. C. (2013). Neuromuscular control of hovering wingbeat kinematics in response to distinct flight challenges in the ruby-throated hummingbird, *Archilochus colubris*. *J. Exp. Biol.* **216**, 4161-4171. doi:10.1242/jeb.089383
- Reiser, P. J., Welch, K. C., Suarez, R. K. and Altshuler, D. L. (2013). Very low force-generating ability and unusually high temperature dependency in hummingbird flight muscle fibers. *J. Exp. Biol.* **216**, 2247-2256. doi:10.1242/jeb.068825
- Robertson, A. M. B. and Biewener, A. A. (2012). Muscle function during takeoff and landing flight in the pigeon (*Columba livia*). *J. Exp. Biol.* **215**, 4104-4114. doi:10.1242/jeb.075275
- Segre, P. S., Dakin, R., Zordan, V. B., Dickinson, M. H., Straw, A. D. and Altshuler, D. L. (2015). Burst muscle performance predicts the speed,

- acceleration, and turning performance of Anna's hummingbirds. *Elife* **4**, 1-23. doi:10.7554/eLife.11159
- Sponberg, S., Libby, T., Mullens, C. H. and Full, R. J.** (2011). Shifts in a single muscle's control potential of body dynamics are determined by mechanical feedback. *Philos. Trans. R. Soc. B Biol. Sci.* **366**, 1606-1620. doi:10.1098/rstb.2010.0368
- Stevenson, R. D. and Josephson, R. K.** (1990). Effects of operating frequency and temperature on mechanical power output from moth flight muscle. *J. Exp. Biol.* **149**, 61-78.
- Syme, D. A.** (2005). Functional properties of skeletal muscle. *Fish Physiol.* **23**, 179-240. doi:10.1016/S1546-5098(05)23006-6
- Syme, D. A. and Josephson, R. K.** (2002). How to build fast muscles: synchronous and asynchronous designs. *Integr. Comp. Biol.* **42**, 762-770. doi:10.1093/icb/42.4.762
- Syme, D. A. and Stevens, E. D.** (1989). Effect of cycle frequency and excursion amplitude on work done by rat diaphragm muscle. *Can. J. Physiol. Pharmacol.* **67**, 1294-1299. doi:10.1139/y89-206
- Tobalske, B. W. and Biewener, A. A.** (2008). Contractile properties of the pigeon supracoracoideus during different modes of flight. *J. Exp. Biol.* **211**, 170-179. doi:10.1242/jeb.007476
- Tobalske, B. W., Peacock, W. L. and Dial, K. P.** (1999). Kinematics of flap-bounding flight in the zebra finch over a wide range of speeds. *J. Exp. Biol.* **202**, 1725-1739.
- Tobalske, B. W., Hedrick, T. L. and Biewener, A. A.** (2003). Wing kinematics of avian flight across speeds. *J. Avian Biol.* **34**, 177-184. doi:10.1034/j.1600-048X.2003.03006.x
- Tobalske, B. W., Warrick, D. R., Clark, C. J., Powers, D. R., Hedrick, T. L., Hyder, G. A. and Biewener, A. A.** (2007). Three-dimensional kinematics of hummingbird flight. *J. Exp. Biol.* **210**, 2368-2382. doi:10.1242/jeb.005686
- Tobalske, B. W., Biewener, A. A., Warrick, D. R., Hedrick, T. L. and Powers, D. R.** (2010). Effects of flight speed upon muscle activity in hummingbirds. *J. Exp. Biol.* **213**, 2515-2523. doi:10.1242/jeb.043844
- Williamson, M. R., Dial, K. P. and Biewener, A. A.** (2001). Pectoralis muscle performance during ascending and slow level flight in mallards (*Anas platyrhynchos*). *J. Exp. Biol.* **204**, 495-507.

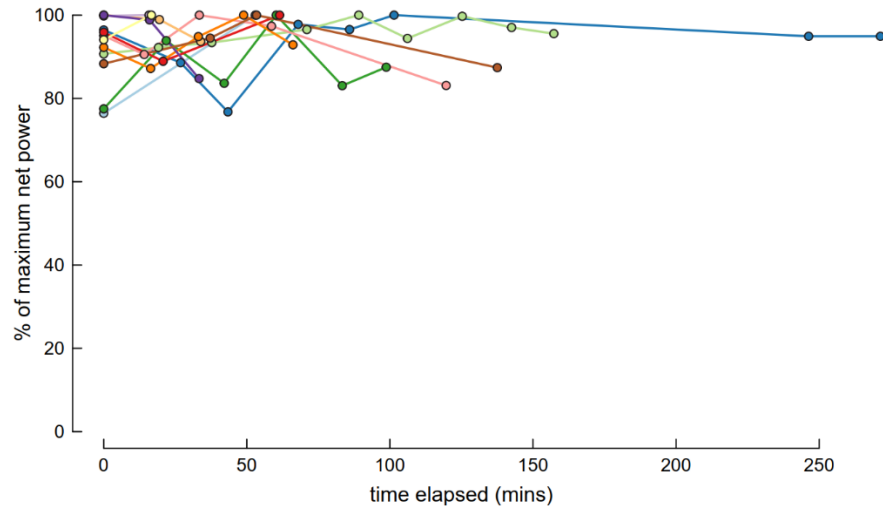


Figure S1. Time course of net power output for each individual bird in the study. A baseline work loop trial (-20% phase, 4 pulse duration, 28Hz frequency, 15% strain) was run between each experimental trial and the net power output of each baseline trial was measured. The net power outputs of all such baseline trials are plotted against the maximum baseline net power on a per-bird basis (colors correspond to individuals). In many cases, experiments could run for several hours with little loss in net power output, as measured via baseline trials.

Table S1. Bird mass, pectoralis muscle mass, and muscle length for the 12 birds in the study. The muscle length short axis of the pectoralis is the shortest length between the center of humeral insertion and the cranial end of the sternum, and the long axis is the length from the humeral attachment to the posterior most attachment on the sternum. Physiological cross-sectional area was obtained as described in the methods. Peak isometric force was measured after the experiments had ended for birds 2-12, unless the muscle had degraded to a level where this measurement was no longer valid. Bird 1 had its peak isometric force measured prior to the experiments. Peak isometric stress is force divided by physiological cross-sectional area.

bird number	bird mass (g)	pectoralis muscle mass (g)	muscle length (mm)		physiological cross-sectional area (cm ²)	peak isometric force (N)	peak isometric stress (N/cm ²)
			short axis	long axis			
1	14.2	1.25	16	28	0.54	10.6	19.63
2	13.1	1.07	15	27	0.48	3.3	6.88
3	13.6	1.46	13	27	0.69	5.4	7.83
4	15.5	1.25	21	30	0.46	5.8	12.61
5	13.5	1.23	18	26	0.51	5.0	9.80
6	13.5	1.19	13	26	0.56	-	-
7	12.9	1.20	14	28	0.54	3.5	6.48
8	13.9	1.12	19	28	0.45	3.3	7.33
9	15.4	1.23	15	27	0.55	-	-
10	15.1	1.27	17	31	0.50	-	-
11	13.1	1.02	13	27	0.53	-	-
12	12.8	1.03	14	29	0.45	-	-

Table S2. The data presented in Figures 3-7 come from 14 experiments for which one parameter was varied and the other parameters were held constant. For each experiment, the varied parameter is indicated in grey with the values given as lower bound – upper bound : interval. We varied amplitude as distance (mm) instead of strain because we were comparing muscle velocity in mm/s. The interval steps varied with amplitude and ranged from 0.042 to 0.07, with an average value of 0.049. The full range of amplitudes represents approximately 13.1-16.8% strain for a mean muscle length of approximately 21 mm. The sample size for each experiment was three or four individuals (biological replicates), and the individual birds are presented in the far-right column. None of the 12 individuals could be used in all experiments.

experiment number	duration (# of pulses)	phase timing (% cycle before peak length)	amplitude (mm)	frequency (Hz)	individual number
1	1-7 : 1	-25	1.58	26	1,4,7
2	1-7 : 1	-25	1.58	28	1,4,7
3	1-7 : 1	-25	1.58	32	1,4,7
4	3	-35 – 10 : 5	1.58	28	2,3,4,6
5	4	-35 – 10 : 5	1.58	28	2,3,4,6
6	5	-35 – 10 : 5	1.58	28	2,3,4,6
7	3	-30	1.38 – 1.76:~0.05	28	2,3,5,8
8	3	-30	1.58	24-32 : 1	2,3,8,12
9	3	-20	1.38 – 1.76:~0.05	28	3,5,8,12
10	3	-20	1.58	24-32 : 1	9,10,11,12
11	4	-30	1.38 – 1.76:~0.05	28	2,3,5,8
12	4	-30	1.58	25-32 : 1	2,3,5,10
13	4	-20	1.38 – 1.76:~0.05	28	2,3,5,8
14	4	-20	1.58	24-32 : 1	9,10,11,12

Table S3. We compared six models to determine which combination of frequency, amplitude, duration (# pulses), and phase best explained variation in net power. The six models are listed by row in ascending order of Deviance Information Criteria (DIC). Parameters of fixed effects, with 95% highest posterior density (HPD) intervals, appear in columns 2 (Frequency) through 10 (Intercept). Bolding indicates that the 95% HPD of that parameter excludes zero. An empty cell indicates that a parameter was not included in a model. Abbreviations: Freq – frequency; Pha – phase; Pul – stimulus pulses; Amp – amplitude; Int – intercept; R² – conditional R²

Model name	Frequency	Amplitude	Pulses	Phase	Freq*Pha	Freq*Pul	Amp*Pha	Amp*Pul	Int	DIC	ΔDIC	R ²
Frequency interactions	-0.321 (-0.390 – -0.254)	0.118 (0.054 – 0.185)	0.372 (0.304 – 0.443)	-0.689 (-0.779 – -0.602)	-0.227 (-0.293 – -0.163)	-0.233 (-0.299 – -0.163)				469.83	0	0.71
All interactions	-0.322 (-0.389 – -0.250)	0.112 (0.036 – 0.187)	0.372 (0.299 – 0.441)	-0.688 (-0.778 – -0.598)	-0.227 (-0.293 – -0.164)	-0.233 (-0.299 – -0.166)	0.018 (-0.064 – 0.093)	0.030 (-0.050 – 0.106)		472.62	2.79	0.71
No interactions	-0.339 (-0.417 – -0.259)	0.120 (0.039 – 0.194)	0.350 (0.263 – 0.435)	-0.675 (-0.789 – -0.571)						568.00	98.18	0.58
Amplitude interactions	-0.339 (-0.418 – -0.260)	0.113 (0.020 – 0.200)	0.351 (0.264 – 0.433)	-0.675 (-0.783 – -0.567)			0.020 (-0.076 – 0.110)	0.028 (-0.064 – 0.117)		571.19	101.36	0.58
No amplitude	-0.339 (-0.422 – -0.260)		0.348 (0.263 – 0.434)	-0.677 (-0.786 – -0.571)						574.71	104.88	0.56
Intercept only									-0.061 (-0.441 – 0.281)	751.01	281.18	0.15

Table S4. Parameters of fixed effects from mixed models fit to the data when duty cycle is used in place of stimulus duration. We compared six models to determine which combination of frequency, amplitude, duty cycle, and phase best explained variation in net power. The six models are listed by row in ascending order of Deviance Information Criteria (DIC). Parameters of fixed effects, with 95% highest posterior density (HPD) intervals, appear in columns 2 (Frequency) through 10 (Intercept). Bolding indicates that the 95% HPD of that parameter excludes zero. An empty cell indicates that a parameter was not included in a model. Abbreviations: Freq – frequency; Pha – phase; DuCy – duty cycle; Amp – amplitude; Int – intercept; R² – conditional R²

Model name	Frequency	Amplitude	Duty cycle	Phase	Freq*Pha	Freq*DuCy	Amp*Pha	Amp*DuCy	Int	DIC	ΔDIC	R ²
Frequency interactions	-0.162 (-0.211 – -0.111)	0.170 (0.06 – 0.275)	-0.118 (-0.168 – -0.068)	-0.752 (-0.802 – -0.704)	-0.124 (-0.219 – -0.036)	-0.125 (-0.169 – -0.084)				750.66	0	0.74
All interactions	-0.159 (-0.209 – -0.109)	0.144 (0.017 – 0.273)	-0.127 (-0.181 – -0.07)	-0.735 (-0.817 – -0.653)	-0.124 (-0.216 – -0.033)	-0.126 (-0.168 – -0.08)	-0.062 (-0.314 – 0.175)	-0.012 (-0.04 – 0.017)		754.24	3.59	0.74
No interactions	-0.128 (-0.178 – -0.08)	0.122 (0.015 – 0.229)	-0.133 (-0.187 – -0.082)	-0.748 (-0.8 – -0.699)						787.58	36.93	0.71
Amplitude interactions	-0.127 (-0.175 – -0.074)	0.101 (-0.034 – 0.225)	-0.136 (-0.191 – -0.079)	-0.730 (-0.815 – -0.648)			-0.069 (-0.33 – 0.177)	-0.004 (-0.035 – 0.025)		791.36	40.70	0.71
No amplitude	-0.132 (-0.182 – -0.083)		-0.127 (-0.177 – -0.075)	-0.747 (-0.797 – -0.696)						791.96	41.30	0.71
Intercept only									0.01 (-0.28 – 0.30)	1300.24	549.58	0.15